Physics and Imaging in Radiation Oncology 26 (2023) 100431

Contents lists available at ScienceDirect

Physics and Imaging in Radiation Oncology

journal homepage: www.sciencedirect.com/journal/physics-and-imaging-in-radiation-oncology

Original Research Article

Deep learning-based segmentation of prostatic urethra on computed tomography scans for treatment planning

Lucía Cubero [a,c], Laura García-Elcano [a], Eugenia Mylona [b], Adrien Boue-Rafle [c], Cesare Cozzarini [d], Maria Giulia Ubeira Gabellini [e], Tiziana Rancati [f], Claudio Fiorino [e], Renaud de Crevoisier [c], Oscar Acosta [c], Javier Pascau [a,g,*]

[a] Departamento de Bioingeniería, Universidad Carlos III de Madrid, Madrid, Spain
[b] Biomedical Research Institute FORTH, Ioannina, Greece
[c] Université Rennes, CLCC Eugène Marquis, Inserm, LTSI - UMR 1099, F-35000 Rennes, France
[d] Department of Radiation Oncology, San Raffaele Scientific Institute - IRCCS, Milan, Italy
[e] Department of Medical Physics, San Raffaele Scientific Institute - IRCCS, Milan, Italy
[f] Science Unit, Fondazione IRCCS Istituto Nazionale dei Tumori, Milan, Italy
[g] Instituto de Investigación Sanitaria Gregorio Marañón, Madrid, Spain

ARTICLE INFO

Keywords:
Prostate cancer radiotherapy
Intraprostatic urethra
Deep learning segmentation
OAR segmentation
Urinary toxicity

ABSTRACT

Background and purpose: The intraprostatic urethra is an organ at risk in prostate cancer radiotherapy, but its segmentation in computed tomography (CT) is challenging. This work sought to: i) propose an automatic pipeline for intraprostatic urethra segmentation in CT, ii) analyze the dose to the urethra, iii) compare the predictions to magnetic resonance (MR) contours.

Materials and methods: First, we trained Deep Learning networks to segment the rectum, bladder, prostate, and seminal vesicles. Then, the proposed Deep Learning Urethra Segmentation model was trained with the bladder and prostate distance transforms and 44 labeled CT with visible catheters. The evaluation was performed on 11 datasets, calculating centerline distance (CLD) and percentage of centerline within 3.5 and 5 mm. We applied this method to a dataset of 32 patients treated with intensity-modulated radiation therapy (IMRT) to quantify the urethral dose. Finally, we compared predicted intraprostatic urethra contours to manual delineations in MR for 15 patients without catheter.

Results: A mean CLD of 1.6 ± 0.8 mm for the whole urethra and 1.7 ± 1.4, 1.5 ± 0.9, and 1.7 ± 0.9 mm for the top, middle, and bottom thirds were obtained in CT. On average, 94% and 97% of the segmented centerlines were within a 3.5 mm and 5 mm radius, respectively. In IMRT, the urethra received a higher dose than the overall prostate. We also found a slight deviation between the predicted and manual MR delineations.

Conclusion: A fully-automatic segmentation pipeline was validated to delineate the intraprostatic urethra in CT images.

1. Introduction

Prostate cancer (PCa) is the most common cancer worldwide in men over 45 years old [1]. Despite its high prevalence, PCa has a survival rate of 98%, all stages combined [2]. Radiation therapy (RT) is one of the primary treatments for PCa, contributing to improved results and survival. However, the exposure of surrounding organs to ionizing radiation has been associated with acute and late adverse events, including urinary, rectal, and sexual toxicities [3].

Recent breakthroughs, including intensity-modulated radiotherapy (IMRT), stereotactic body radiotherapy (SBRT), and image-guided radiotherapy (IGRT), have enabled more precise tumor targeting while better sparing nearby organs at risk (OARs). Nonetheless, the intraprostatic urethra, which transverses the prostate gland, is inevitably exposed to the maximum delivered dose. Emerging dose escalation protocols, ranging from moderate to extreme hypofractionation, may increase disease control; however, they may also cause degeneration and tissue necrosis in urethral structures [3,4]. As a result of RT-induced

* Corresponding author at: Departamento de Bioingeniería, Universidad Carlos III de Madrid, Madrid, Spain.
E-mail address: jpascau@ing.uc3m.es (J. Pascau).

https://doi.org/10.1016/j.phro.2023.100431
Received 15 November 2022; Received in revised form 8 March 2023; Accepted 14 March 2023
Available online 21 March 2023

urethral injury, acute and late symptoms arise, including dysuria, hematuria, nocturia, and urinary incontinence [5,6].

Urethra-sparing techniques and dose constraints have been proposed for reducing the risk of long-term genitourinary toxicities [7–9], but require accurate segmentation of the intraprostatic urethra. However, this structure is entirely invisible on the planning computed tomography (CT) images due to the lack of contrast between the urethra and prostate [10,11]. A Foley catheter, an indwelling catheter used to drain the urine, is typically inserted to allow detection of the urethra but is invasive producing patient discomfort, is inconvenient for daily routine practice and can damage the urethra [12]. Besides, its placement may shift the actual urethral position [13].

Only a few studies have attempted to segment the prostatic urethra in planning CT images. Initially, surrogate models were used to estimate the urethra location relative to the prostate midplane based on empirical assumptions [10,14]. Multi-atlas-based segmentation methods using deformable image registration were able to better approximate the position of the prostatic urethra [15,16], but computation times hamper their application in routine clinical practice.

Recently, Deep Learning (DL) algorithms have shown their potential to revolutionize prostate cancer diagnosis, prognosis, and treatment [17]. In diagnostic imaging, DL models have demonstrated state-of-the-art performance for automating segmentation tasks, including prostate cancer RT-relevant structures [18–20]. Meyer et al. [20] developed a semi-supervised domain adaptation pipeline for segmenting the prostate and other structures, including the neurovascular bundles and external urethral sphincter. In another study [21], the distal prostatic urethra and zonal anatomy of the prostate were segmented through a multi-class segmentation. To the best of our knowledge, DL-based models have never been used for the automatic segmentation of the intraprostatic urethra from CT scans.

Segmenting the urethra is important for i) prostate RT planning, ii) dosimetric analysis, iii) toxicity prediction. The main hypothesis in this study is that DL models can surpass the existing state-of-the-art atlas-based algorithms for intraprostatic urethra segmentation both in terms of accuracy and computation time. With this aim, we propose a DL-based pipeline for efficiently and accurately estimating the intraprostatic urethra. The proposed method exploits bladder and prostate contours to anatomically guide the model, which learns the location of the urethra directly from computed Euclidean Distance Maps. The framework was trained and evaluated on a previously published CT database [15]. Since the method depends only on the OAR contours, we also analyzed the feasibility of segmenting the urethra from MR images.

2. Materials and methods

2.1. Proposed pipeline

Fig. 1 depicts the proposed workflow (freely available at https://github.com/BSEL-UC3M/DLUS). First, Localization Network predicts a coarse prostate segmentation from the CT and generates a volume of interest (VOI) of 224x224x224 voxels centered on the generated contour. This VOI is the input to OARs Segmentation Network, which predicts the delineations of the rectum, bladder, prostate, and seminal vesicles. These binary contours are finally used to generate the Euclidean Distance Maps, which are the input to Deep Learning Urethra Segmentation (DLUS) Network to delineate the intraprostatic urethra.

The following sections will describe the databases employed to train each network, and its architecture and parameters. All the experiments were performed on a CUDA-enabled Nvidia Quadro RTX 8000 GPU with 48 GB RAM. DL models were implemented in PyTorch 1.11.

2.1.1. Databases

Data were gathered from four different databases (Table 1) in the context of a European research consortium (PerPlanRT) supervised by ethics committees ensuring all patients had given prior consent for data sharing. Databases UryTOX [6,15], INT [22], and IHU [23,24] were used to train Localization and OARs Segmentation Networks, comprising a total of 351 patients treated with IMRT. Data included CT scans and manual ground truth delineations for the rectum, bladder, prostate, and seminal vesicles. On the other hand, 55 CT scans from MABUS dataset [15] were employed to train DLUS framework. This database comprised CT and manual delineations for the bladder, prostate, and intraprostatic urethra via Foley catheter.

2.1.2. Localization and OARs segmentation

To train Localization and OARs Segmentation Networks, 351 images from the three databases were divided into train (278) and test (73) following a random 80:20 division. Models were trained (tested) with 120 (34), 62 (15), and 96 (24) datasets from UryTOX, INT, and IHU.

First, Localization Network was trained to generate a coarse prostate segmentation, from which a VOI centered on this organ was created. This model was implemented with a modified 3D U-Net [25], using as inputs the CT image and manual prostate segmentation resized to 128x128x128. The network was trained with a batch size of 2 for 500 epochs, weighted cross entropy loss assigning weights of 0.1 and 1 to the background and prostate, Adam optimizer with a learning rate of 10^{-3}, and He normal initializer, which draws the weights randomly from a

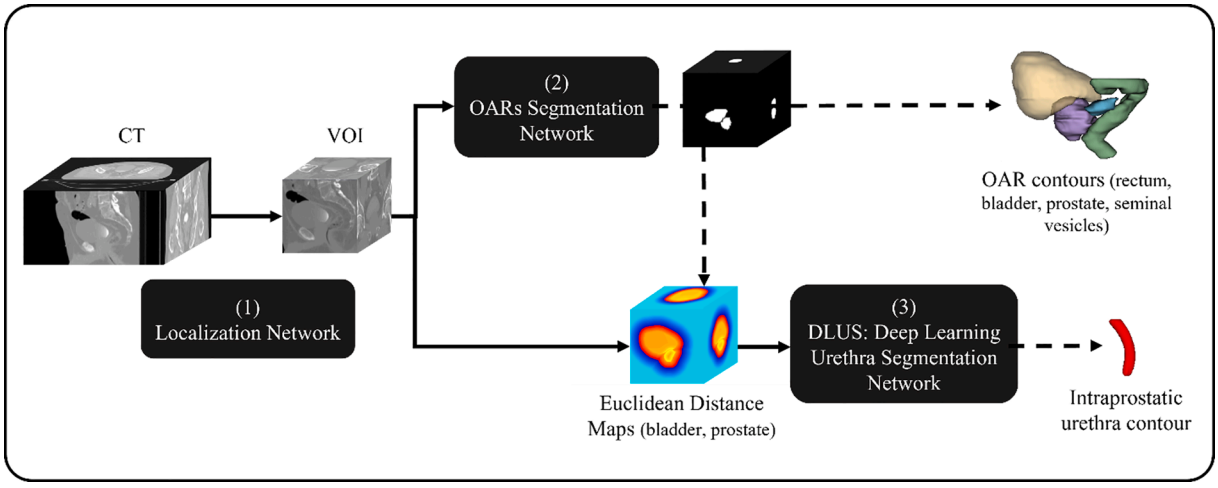

Fig. 1. Proposed framework. First, the *Localization Network* localizes the volume of interest centered on the prostate. Then, the *OARs Segmentation Network* automatically segments the four OARs (rectum, bladder, prostate, and seminal vesicles). Finally, the predicted binary contours are used to generate the Euclidean Distance Maps, which serve as the input to the *Deep Learning Urethra Segmentation Network* to segment the intraprostatic urethra.

Table 1
Specifications of the three databases for OAR segmentation (UryTOX, INT, IHU) and the database for intraprostatic urethra segmentation (MABUS).

	Name	Center	CT images (n)	RT treatment	Image dimensions (X Y Z pixels) Pixel size (XY Z mm)
OAR segmentation	UryTOX	CLCC Eugène Marquis (France)	154	IMRT/IGRT	512 512 (84 ~ 189) (1.008 ~ 1.172) (2 ~ 3)
	INT	Istituto Nazionale dei Tumori (Italy)	77	IMRT/IGRT	512 512 (94 ~ 263) (0.977 ~ 1.172) (2 ~3)
	IHU	San Raffaele Scientific Institute (Italy)	120	IMRT/IGRT	512 512 (55 ~ 115) (0.826 ~ 0.977) (1.626 ~ 3)
Urethra segmentation	MABUS	CLCC Eugène Marquis (France)	55	Brachytherapy	512 512 48 0.633 3

truncated normal distribution accounting for the previous neuronal layer's size.

Then, OARs Segmentation Network was trained to predict a fine delineation of the four OARs. It was trained with nnU-Net [26], a DL-based self-configuring framework. For a new given task, this method automatically optimizes all the steps for segmentation: preprocessing, network architecture, training parameters, and post-processing. We trained a 3D full-resolution U-Net within this framework with 5-fold cross-validation for 500 epochs per fold. We used the CT VOIs and multi-class masks englobing the four OARs manual contours as inputs. The model was trained with a combination of Dice and Cross-Entropy losses and Adam optimizer with a learning rate of 10^{-4}.

The trained OARs Segmentation Network was evaluated in the multi-institutional test set measuring Dice Score Coefficient (DSC) and Average Surface Distance (ASD) between manual and predicted segmentations. The DSC was also computed independently for each institution's test data to analyze if the model was underperforming in any database due to differences in segmentation protocol. For two binary volumes V_1 and V_2, the DSC is the relative spatial overlap between V_1 and V_2 [27]; whereas the ASD is the average of all the Euclidean distances between the boundary voxels of V_1 and V_2 [28].

Localization and OARs Segmentation Networks provided a fully-automatic pipeline. However, to obtain the intraprostatic urethra (as described in the following section), manual contours of the bladder and prostate could also be used if available, skipping these two first steps.

2.1.3. Intraprostatic urethra segmentation

The development of Deep Learning Urethra Segmentation (DLUS) Network was similar to the work of Balagopal et al. (2021) [29], in which they segmented the Clinical Target Volume in post-operative prostate RT patients using the Euclidean distances between neighboring organs.

In a first attempt, we trained DLUS with binary masks, expecting that it would learn the spatial relationships between the urethra and other OARs. This yielded a low accuracy, since the model was not able to learn this geometrical information from the binary masks. To improve the segmentation, we trained the network on Euclidean distance transforms for each predicted segmentation of the bladder and prostate. For each organ, we computed two distance maps, i) from its centroid to the boundaries (zero in the centroid and higher closer to the boundary), ii) from the boundary (zero values) to the pixels outside the organ (the further, the more negative). The Euclidean distance transform was also computed for the joint bladder and prostate masks. The final distance maps were obtained as the sum of three distance transforms: joint prostate and bladder, prostate, and weighted bladder (voxel weight depending on its distance to the prostate: the closer the higher). We also tested the performance of a model with a Laplacian distance map, obtaining less accurate results with longer computational times.

To train DLUS nnU-Net network, MABUS database was randomly divided into train and test following 80:20 partitions, resulting in 44 train and 11 test cases. nnU-Net was trained with a 3D full-resolution U-Net with 5-fold cross-validation for 500 epochs per fold. As inputs, we used the combined distance maps and ground truth segmentations of the urethra. DLUS was trained with a combination of Dice and Cross-Entropy losses and Adam optimizer with a learning rate of 10^{-4}.

The predicted urethra contours were evaluated with the Centerline Distance (CLD), Percentage of Centerline Points (PWR), and time needed to obtain the segmentation. The centerline was computed as a 3D cubic spline curve of equidistant points describing the urethra within the prostate. The CLD was the average of the differences between the predicted and ground truth urethral centerlines. It was computed for the whole segmented path and each region after dividing the ground truth central path into three equivalent segments from the apex to the base (top, medium, and bottom regions). The PWR was calculated as the percentage of segmented centerline lying within a radius of 3.5 mm and 5 mm around the ground truth centerline.

2.2. Study of the dosimetric impact

An independent series of 32 prostate cancer patients treated with 78/80 Gy IMRT was employed in an illustrative dosimetric study to analyze if the urethra had received a higher dose than the whole prostate during treatment. This database included the CT and manually-delineated rectum, bladder, prostate, and seminal vesicles. First, we automatically segmented the intraprostatic urethra with DLUS. Then, doses within the urethra and prostate volumes were obtained from the 3D planning dose distribution and compared in terms of Dose Volume Histograms (DVHs) and minimum dose delivered to 95% of the prostate (D95).

2.3. Validation on MR data

The main criticism of urethra segmentation methods trained on CT images with a Foley catheter is the possible shift in the urethra position [13]. To analyze if our predicted contours were too different from the position of catheter-free urethras, we validated our methodology on 15 MR images without catheter where the urethra had been manually delineated in the same medical institution as MABUS database (Table 1).

CT scans from similar dates were available for the 15 patients. MR and CT images were non-rigidly registered with MIMFUSION (MIM Software Inc., Ohio, United States), allowing the transfer of manual urethra contours from MR to CT. Then, the same steps as defined in Fig. 1 were followed. The manual and predicted delineations were compared by computing the CLD and PWR within 3.5 and 5 mm.

3. Results

3.1. OARs segmentation

Table 2 shows the evaluation of OARs Segmentation Network. The average DSCs for the rectum, bladder, prostate, and seminal vesicles were 86.3%, 93.6%, 83.3%, and 70.0%, respectively. All predicted segmentations obtained an ASD below 2 mm. Between the three databases, the most substantial differences appeared in the prostate, for which the model slightly underperformed with IHU data (DSC = 80.4%). For the seminal vesicles, the results obtained for UryTOX (DSC = 72.5%)

Table 2
Evaluation results (Dice Score Coefficient (DSC) and Average Surface Distance (ASD)) between the predicted segmentations obtained with the OARs Segmentation Network and the ground truth contours. The DSC is also depicted for each individual database.

Database		Rectum	Bladder	Prostate	Seminal Vesicles
UryTOX (n = 34)	DSC (%)	**86.7 ± 5.2**	94.0 ± 2.3	84.2 ± 5.6	**72.5 ± 10.9**
INT (n = 15)	DSC (%)	85.1 ± 6.7	**96.0 ± 2.2**	**85.9 ± 9.7**	68.0 ± 9.9
IHU (n = 24)	DSC (%)	86.4 ± 4.7	91.5 ± 7.7	80.4 ± 6.7	67.7 ± 11.1
Average (n = 73)	DSC (%)	86.3 ± 5.4	93.6 ± 5.0	83.3 ± 7.3	70.0 ± 11.0
	ASD (mm)	1.44 ± 1.11	0.95 ± 0.37	1.63 ± 0.63	1.76 ± 1.20

were superior to both INT and IHU databases (DSC $\leq$ 68.0%).

3.2. Urethra segmentation

The performance of DLUS was superior to the state-of-the-art multi-atlas approach [15] (Table 3a). This was a direct comparison, as the same data were evaluated. However, the results for the multi-atlas approach corresponded to a leave-one-out cross-validation (n = 1), while DLUS was evaluated on a test set with 11 images to avoid over-fitting and ensure more robust results. With DLUS, the CLD in the whole urethra was 1.6 mm, compared to the 3.3 mm with multi-atlas. The PWR within 5 mm also improved from 53% to 97%. Moreover, our method was 20 times faster: the urethra contour was calculated in 1.8 min, compared to more than 35 min for the multi-atlas approach (running on i7-8700 workstation with 32 GB RAM). Fig. 2 shows the best and worst segmented cases.

3.3. Dosimetric impact

The calculated D95 and DVHs for the prostate and intraprostatic urethra predicted volumes differed. This showed that the urethra received a statistically significant (p = 0.019) higher dose than the whole prostate (Fig. 3).

3.4. Validation on MR data

After an initial assessment, we excluded two patients from the evaluation as their CLD was above 10 mm; therefore, we considered that the model failed to segment them. The evaluation was performed for the remaining 13 patients. We observed a mismatch in the last part of the urethra between some predictions and their corresponding ground truth contours, probably due to the differences between the urethra and prostate in MR and CT. We post-processed our predicted urethra contours by removing the slices outside the prostate segmentation. The CLD and PWR within 5 mm revealed a worse performance when using the MR contours (3.9 mm and 62.3%, respectively) compared to CT (1.6 mm and 97.4%, Table 3b). Our results are closer to those from Belue et al. (2022) [30], who trained a 3D U-Net model with 798 T2-weighted MR images obtaining a CLD of 2.6 mm on 140 test MR scans.

4. Discussion

In this paper, we proposed a fully automatic DL-based methodology to segment OARs and intraprostatic urethra in CT for prostate cancer RT, comparing our results with the previous baseline approach and with manual segmentations on MR.

Our automatic OARs segmentation facilitates the workflow's implementation into the clinical setting. If we compare our DSC results (Table 2) for rectum, bladder and prostate (86.3%, 93.6%, 83.3%) to previous works [31–34] (best in [32] 84.0%, 95.0%, 90.0%), the only organ with more than 5% difference is the prostate. This is probably explained by the clinical and multicentric origin of our databases, with segmentations that have not been curated. In the case of the seminal vesicles, only [31] has reported a DSC of 70.1% on this region, equivalent to our DSC of 70.0%. These results show how our automatic OARs segmentation could replace manual contouring as a previous step for automatic urethra prediction.

Our DLUS approach does not require any catheter to estimate the position of the urethra, as it uses the OARs distance maps to guide the delineation. Segmenting and reporting the dose to the urethra is important for studying its involvement in toxicity studies, but also to conduct personalized plannings with reduced radio-induced toxicity and improved tumor control, which is feasible with the new highly conformal intensity-modulated irradiation systems [35]. Our analysis on predicted urethra contours showed that it received a higher dose during treatment than the whole prostate (Fig. 3), depicting the importance of considering the urethra as an independent organ in prostate RT, since several authors have shown that a high dose to the urethra increases the risk of long-term genitourinary toxicities [7–9].

When compared to the reference multi-atlas-based approach on the same database, the CDL decreased from 3.3 mm to 1.6 mm, demonstrating the superiority of our framework in accuracy and computational requirements, which are tightly related to clinical integration feasibility. Even if these results are favorable, the urethra in the reference database was contoured via Foley catheter delineation, which could imply a deviation from the anatomical position. The results obtained when applying the whole workflow to 15 CTs with urethra position obtained from MR increased the CLD to 3.8 mm. PWR was also smaller: 93.6% vs 46.7% within 3.5 mm, and 97.4% vs 62.3% within 5 mm. These values indicate that the intraprostatic urethra had possibly been slightly displaced by the catheter. Nonetheless, other error sources could justify this disagreement: the registration inaccuracy and the bladder filling difference between CT and MR images of the same patient.

A recently published study where the urethra was segmented with a 3D UNet trained only with MR data [30] obtained a CLD of 2.6 mm over the whole urethra. This value falls between our metrics on CT and MR data, showing that the urethra is a complex organ to segment even in MR. Nonetheless, we had to exclude two MR images from this evaluation

Table 3
Comparative results (Central Line Distance (CLD), Percentage of Centerline Points (PWR), and computation time) between the predicted and ground truth contours. The first two methods (MABUS multi-atlas approach [15] and DLUS) were trained with manual delineations performed on CT. The following approach only with MR data (Belue et al. [30]). The last one corresponds to the evaluation of DLUS when comparing against manual contours delineated on MR images.

		CLD (mm)				PWR (%)		Time
		Whole	Top	Middle	Bottom	<3.5 mm	<5mm	(min)
(a) CT	MABUS [15] (n = 1)	3.3 ± 1.2	3.7 ± 1.7	2.5 ± 1.6	3.0 ± 1.8	53 ± 29	53 ± 29	>35
	DLUS (n = 11)	1.6 ± 0.8	1.7 ± 1.4	1.5 ± 0.9	1.7 ± 0.9	93.6 ± 12.4	97.4 ± 8.2	1.8
(b) MR	Belue et al. [30] (n = 140)	2.6 ± 1.3	3.7 ± 2.6	2.3 ± 1.4	1.5 ± 1.0	–	–	–
	DLUS (n = 13)	3.9 ± 1.3	3.9 ± 2.1	3.9 ± 1.8	3.3 ± 1.4	46.7 ± 28.4	62.3 ± 26.9	1.8

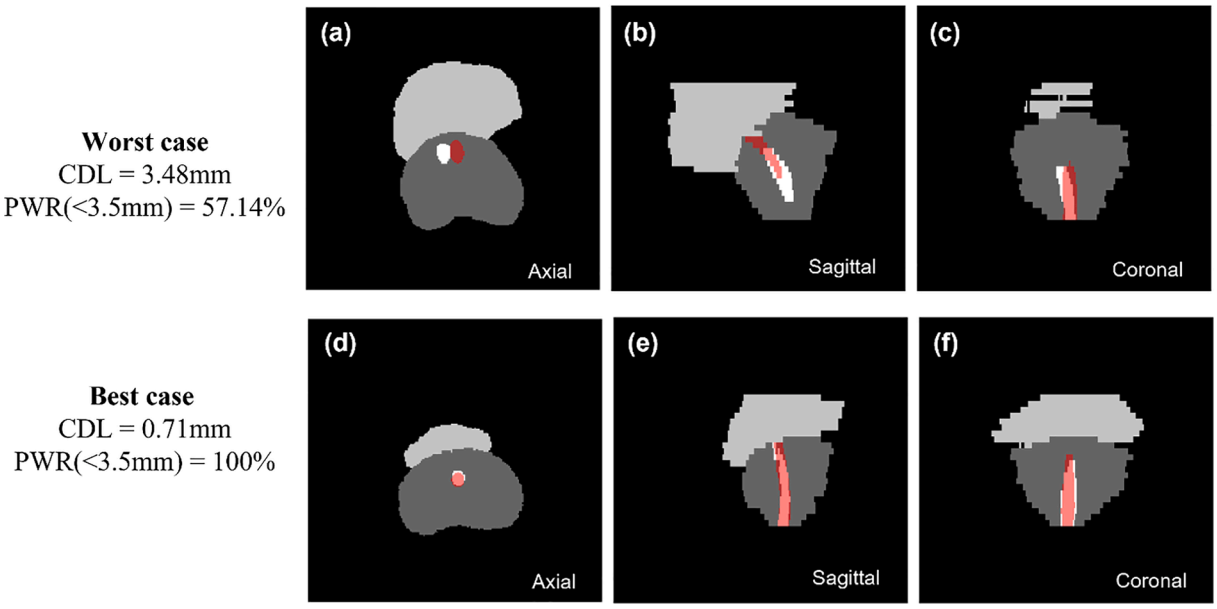

Fig. 2. Visual comparison and evaluation metrics between the manually delineated ground truth urethra (white) and the predicted segmentation with the proposed method (red) for the worse case (a)-(c) and the best case (d)-(f). (For interpretation of the references to colour in this figure legend, the reader is referred to the web version of this article.)

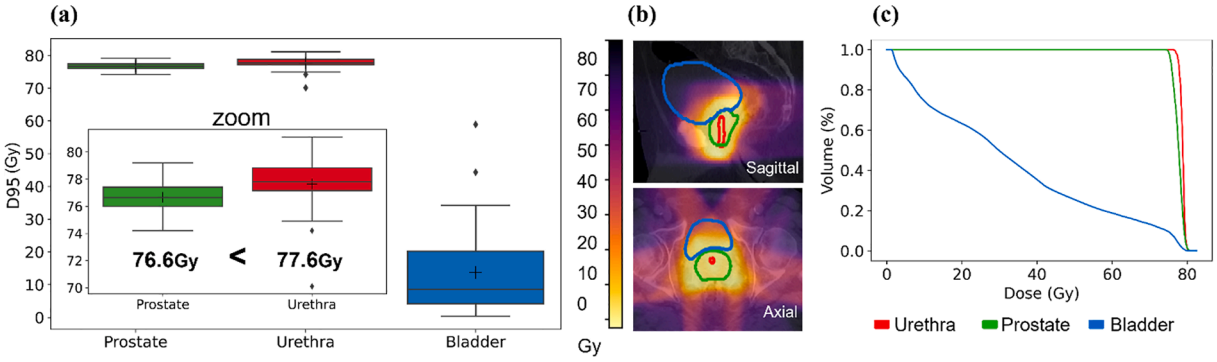

Fig. 3. Results of the dose-volume analysis. (a) shows the box plot of D95 values for the bladder, the prostate, and the urethra, (b) depicts the areas of the OARs receiving the dose for an example patient, (c) represents the DVH curves of those OARs for an example patient.

as their CLD was above 10 mm, indicating that our model was unable to segment these cases. One explanation for this underperformance could be the presence of tumors close to the urethra, pushing the structure to one of the sides of the prostate and inducing a geometrical asymmetry. Belue et al. (2022) [30] also found that asymmetric cases were more challenging to segment.

DLUS was successfully validated with both catheter-guided and catheter-free urethras. Its main advantage is that it only uses the contours of the bladder and prostate to generate their Euclidean distance maps and guide the urethral segmentation. The slight underperformance of DLUS when tested on MR-delineated urethras would possibly be solved by retraining our workflow with manual MR contours. Even if RT is moving towards MR-guided treatments, most medical centers still depend on planning CTs to calculate the estimated dose in the OARs and urethra, which supports the clinical need of our framework.

One limitation of this study is that the presence of the catheter in the training images might have slightly modified the real anatomy of the urethra. To mitigate this effect, we evaluated the methodology by computing the CLD and PWR. Other factors have to be further studied, such as position changes in the urethra for different bladder-filling situations or the introduction of uncertainty maps to improve confidence in the results.

In conclusion, this study validated a fully-automatic pipeline to estimate the intraprostatic urethra in CT and MR images. The methodology outperformed previous approaches, opening the option to include the urethra as an independent organ in prostate cancer treatment plans, which could reduce long-term toxicity for the patients.

Declaration of Competing Interest

The authors declare that they have no known competing financial interests or personal relationships that could have appeared to influence the work reported in this paper.

Acknowledgements

Research supported by projects PI18/01625, AC20/00102 and AC20/00123 (Ministerio de Ciencia, Innovación y Universidades, Instituto de Salud Carlos III, Asociación Española Contra el Cáncer and European Regional Development Fund “Una manera de hacer Europa”), TED2021-129392B-I00 (MCIN/AEI/10.13039/501100011033 and European Union “NextGenerationEU”/PRTR) and PerPlanRT (ERA Permed). GPUs were donated by NVIDIA Applied Research Accelerator Program.

Use of medical data.

The use of each medical database for this research was allowed by the corresponding Institutional Review Board and the Consortium Agreement in the EraPerMed project PerPlanRT.

References

[1] Estimated number of new cases in 2020, World, males, ages 45+ (excl. NMSC). Cancer Today. International Agency for Research on Cancer World Health Organization n.d. https://gco.iarc.fr/today/ (accessed September 17, 2022).

[2] Siegel RL, Miller KD, Fuchs HE, Jemal A. Cancer statistics, 2022. CA Cancer J Clin 2022;72:7–33. https://doi.org/10.3322/caac.21708.

[3] Martinez AA, Gonzalez J, Ye H, Ghilezan M, Shetty S, Kernen K, et al. Dose Escalation Improves Cancer-Related Events at 10 Years for Intermediate- and High-Risk Prostate Cancer Patients Treated With Hypofractionated High-Dose-Rate Boost and External Beam Radiotherapy. Int J Radiat Oncol Biol Phys 2011;79:363–70. https://doi.org/10.1016/j.ijrobp.2009.10.035.

[4] Marks LB, Carroll PR, Dugan TC, Anscher MS. The response of the urinary bladder, urethra, and ureter to radiation and chemotherapy. Int J Radiat Oncol Biol Phys 1995;31:1257–80. https://doi.org/10.1016/0360-3016(94)00431-J.

[5] Peeters STH, Heemsbergen WD, van Putten WLJ, Slot A, Tabak H, Mens JW, et al. Acute and late complications after radiotherapy for prostate cancer: Results of a multicenter randomized trial comparing 68 Gy to 78 Gy. Int J Radiat Oncol Biol Phys 2005;61:1019–34. https://doi.org/10.1016/j.ijrobp.2004.07.715.

[6] Mylona E, Acosta O, Lizee T, Lafond C, Crehange G, Magné N, et al. Voxel-Based Analysis for Identification of Urethrovesical Subregions Predicting Urinary Toxicity After Prostate Cancer Radiation Therapy. Int J Radiat Oncol Biol Phys 2019;104:343–54. https://doi.org/10.1016/j.ijrobp.2019.01.088.

[7] Greco C, Pares O, Pimentel N, Louro V, Nunes B, Kociolek J, et al. Urethra Sparing With Target Motion Mitigation in Dose-Escalated Extreme Hypofractionated Prostate Cancer Radiotherapy: 7-Year Results From a Phase II Study. Front Oncol 2022;12:863655. https://doi.org/10.3389/fonc.2022.863655.

[8] Zilli T, Achard V, Le Guevelou J. Intraprostatic Urethra: The New Kid on the Block for Prostate Cancer Radiation Therapy? Int J Radiat Oncol Biol Phys 2022;113:92–5. https://doi.org/10.1016/j.ijrobp.2022.01.022.

[9] Leeman JE, Chen Y-H, Catalano P, Bredfeldt J, King M, Mouw KW, et al. Radiation Dose to the Intraprostatic Urethra Correlates Strongly With Urinary Toxicity After Prostate Stereotactic Body Radiation Therapy: A Combined Analysis of 23 Prospective Clinical Trials. Int J Radiat Oncol Biol Phys 2022;112:75–82. https://doi.org/10.1016/j.ijrobp.2021.06.037.

[10] Waterman FM, Dicker AP. Determination of the urethral dose in prostate brachytherapy when the urethra cannot be visualized in the postimplant CT scan. Med Phys 2000;27:448–51. https://doi.org/10.1118/1.598912.

[11] Yoshimura T, Nishioka K, Hashimoto T, Fujiwara T, Ishizaka K, Sugimori H, et al. Visualizing the urethra by magnetic resonance imaging without usage of a catheter for radiotherapy of prostate cancer. Phys Imaging Radiat Oncol 2021;18:1–4. https://doi.org/10.1016/j.phro.2021.03.002.

[12] Repka MC, Guleria S, Cyr RA, Yung TM, Koneru H, Chen LN, et al. Acute Urinary Morbidity Following Stereotactic Body Radiation Therapy for Prostate Cancer with Prophylactic Alpha-Adrenergic Antagonist and Urethral Dose Reduction. Front Oncol 2016:6. https://doi.org/10.3389/fonc.2016.00122.

[13] Litzenberg DW, Muenz DG, Archer PG, Jackson WC, Hamstra DA, Hearn JW, et al. Changes in prostate orientation due to removal of a Foley catheter. Med Phys 2018;45:1369–78. https://doi.org/10.1002/mp.12830.

[14] Bucci J, Spadinger I, Hilts M, Sidhu S, Smith C, Keyes M, et al. Urethral and periurethral dosimetry in prostate brachytherapy: is there a convenient surrogate? Int J Radiat Oncol Biol Phys 2002;54:1235–42. https://doi.org/10.1016/S0360-3016(02)03054-7.

[15] Acosta O, Mylona E, Le Dain M, Voisin C, Lizee T, Rigaud B, et al. Multi-atlas-based segmentation of prostatic urethra from planning CT imaging to quantify dose distribution in prostate cancer radiotherapy. Radiother Oncol 2017;125:492–9. https://doi.org/10.1016/j.radonc.2017.09.015.

[16] Takagi H, Kadoya N, Kajikawa T, Tanaka S, Takayama Y, Chiba T, et al. Multi-atlas–based auto-segmentation for prostatic urethra using novel prediction of deformable image registration accuracy. Med Phys 2020;47:3023–31. https://doi.org/10.1002/mp.14154.

[17] Goldenberg SL, Nir G, Salcudean SE. A new era: artificial intelligence and machine learning in prostate cancer. Nat Rev Urol 2019;16:391–403. https://doi.org/10.1038/s41585-019-0193-3.

[18] Wang S, He K, Nie D, Zhou S, Gao Y, Shen D. CT male pelvic organ segmentation using fully convolutional networks with boundary sensitive representation. Med Image Anal 2019;54:168–78. https://doi.org/10.1016/j.media.2019.03.003.

[19] Dai Z, Carver E, Liu C, Lee J, Feldman A, Zong W, et al. Segmentation of the Prostatic Gland and the Intraprostatic Lesions on Multiparametic Magnetic Resonance Imaging Using Mask Region-Based Convolutional Neural Networks. Adv Radiat Oncol 2020;5:473–81. https://doi.org/10.1016/j.adro.2020.01.005.

[20] Meyer A, Mehrtash A, Rak M, Bashkanov O, Langbein B, Ziaei A, et al. Domain adaptation for segmentation of critical structures for prostate cancer therapy. Sci Rep 2021;11:11480. https://doi.org/10.1038/s41598-021-90294-4.

[21] Meyer A, Rakr M, Schindele D, Blaschke S, Schostak M, Fedorov A, et al. IEEE 16th Int Symp Biomed Imaging (ISBI). Venice, Italy 2019;2019:696–700. https://doi.org/10.1109/ISBI.2019.8759572.

[22] Mylona E, Cicchetti A, Rancati T, Palorini F, Fiorino C, Supiot S, et al. Local dose analysis to predict acute and late urinary toxicities after prostate cancer radiotherapy: Assessment of cohort and method effects. Radiother Oncol 2020;147:40–9. https://doi.org/10.1016/j.radonc.2020.02.028.

[23] Sini C, Fiorino C, Perna L, Noris Chiorda B, Deantoni CL, Bianchi M, et al. Dose–volume effects for pelvic bone marrow in predicting hematological toxicity in prostate cancer radiotherapy with pelvic node irradiation. Radiother Oncol 2016;118:79–84. https://doi.org/10.1016/j.radonc.2015.11.020.

[24] Bresolin A, Garibaldi E, Faiella A, Cante D, Vavassori V, Waskiewicz JM, et al. Predictors of 2-Year Incidence of Patient-Reported Urinary Incontinence After Post-prostatectomy Radiotherapy: Evidence of Dose and Fractionation Effects. Front Oncol 2020;10:1207. https://doi.org/10.3389/fonc.2020.01207.

[25] Çiçek Ö, Abdulkadir A, Lienkamp SS, Brox T, Ronneberger O. 3D U-Net: Learning Dense Volumetric Segmentation from Sparse Annotation. Med Image Comput Comput Assist Interv (MICCAI) 2016;9901:424–32. https://doi.org/10.1007/978-3-319-46723-8_49.

[26] Isensee F, Petersen J, Klein A, Zimmerer D, Jaeger PF, Kohl S, et al. nnU-Net: Self-adapting Framework for U-Net-Based Medical Image Segmentation. Nat Methods 2021;18:203–11. https://doi.org/10.1038/s41592-020-01008-z.

[27] Dice LR. Measures of the Amount of Ecologic Association Between Species. Ecology 1945;26:297–302. https://doi.org/10.2307/1932409.

[28] Yeghiazaryan V, Voiculescu I. An overview of current evaluation methods used in medical image segmentation. University of Oxford; 2015.

[29] Balagopal A, Nguyen D, Morgan H, Weng Y, Dohopolski M, Lin M-H, et al. A deep learning-based framework for segmenting invisible clinical target volumes with estimated uncertainties for post-operative prostate cancer radiotherapy. Med Image Anal 2021;72:102101. https://doi.org/10.1016/j.media.2021.102101.

[30] Belue MJ, Harmon SA, Patel K, Daryanani A, Yilmaz EC, Pinto PA, et al. Development of a 3D CNN-based AI Model for Automated Segmentation of the Prostatic Urethra. Acad Radiol 2022;29:1404–12. https://doi.org/10.1016/j.acra.2022.01.009.

[31] Schreier J, Genghi A, Laaksonen H, Morgas T, Haas B. Clinical evaluation of a full-image deep segmentation algorithm for the male pelvis on cone-beam CT and CT. Radiother Oncol 2020;145:1–6. https://doi.org/10.1016/j.radonc.2019.11.021.

[32] Balagopal A, Kazemifar S, Nguyen D, Lin M-H, Hannan R, Owrangi A, et al. Fully automated organ segmentation in male pelvic CT images. Phys Med Biol 2018;63:245015. https://doi.org/10.1088/1361-6560/aaf11c.

[33] Kearney V, Chan JW, Wang T, Perry A, Yom SS, Solberg TD. Attention-enabled 3D boosted convolutional neural networks for semantic CT segmentation using deep supervision. Phys Med Biol 2019;64:135001. https://doi.org/10.1088/1361-6560/ab2818.

[34] He K, Cao X, Shi Y, Nie D, Gao Y, Shen D. Pelvic Organ Segmentation Using Distinctive Curve Guided Fully Convolutional Networks. IEEE Trans Med Imaging 2019;38:585–95. https://doi.org/10.1109/TMI.2018.2867837.

[35] Spohn SKB, Sachpazidis I, Wiehle R, Thomann B, Sigle A, Bronsert P, et al. Influence of Urethra Sparing on Tumor Control Probability and Normal Tissue Complication Probability in Focal Dose Escalated Hypofractionated Radiotherapy: A Planning Study Based on Histopathology Reference. Front Oncol 2021;11:652678. https://doi.org/10.3389/fonc.2021.652678.